This is a peer-reviewed, accepted author manuscript of the following research article: Umar, A., Neagu, D., & Irvine, J. T. S. (2023). Renewable syngas & hydrogen synthesis via steam reforming of glycerol over ceria-mediated exsolved metal nano catalysts. International Journal of Hydrogen Energy, 48(70), 27137-27150. https://doi.org/10.1016/j.ijhydene.2023.03.385

Renewable Syngas & Hydrogen Synthesis via Steam Reforming of Glycerol over Ceria-Mediated Exsolved Metal Nano Catalysts

Ahmed Umar[1], Dragos Neagu and John T.S. Irvine
School of Chemistry, University of St Andrews,
North Haugh, St Andrews, Fife KY16 9ST, UK.

Abstract

Currently, catalyst design and development has drawn much attention as results of its strategic importance in the area of energy applications particular those involving biomass conversion. This work tailored exsolution of metal catalysts through the use of ceria for enhanced structural and catalytic behaviour in steam reforming of glycerol. Aside the understanding that defects due to A-site deficiency facilitates the formation of vacant sites and exsolution of metal catalysts on the B-site of perovskite systems, this work has exemplified that metals such as ceria significantly influences the exsolution and general morphological surface architecture and catalytic behaviour. The exsolved nickel catalysts anchored and socketed on the titanate support and the ceria's basic surface properties and oxygen storage-release behaviour has modified the perovskite surface chemistry and enhanced catalytic behaviour particularly deactivation due to carbon deposition and reusability. other exsolvable dopant metal species such as Fe and Co forms alloys with nickel on the surface and the synergy between the dopant metals in the alloy yielded better results. Furthermore, in one of the catalyst systems, the most commonly observed tolerable A-site deficiency and doping limit of 2% known for $SrTiO_3$ perovskite was overstretched by 0.5% (2.5%) thereby increasing the defect chemistry. The catalyst system with such formulation has shown a dramatic exsolution phenomenon and catalytic behaviour and robust suppression of coke. CO selectivity >60% and H_2 selectivity >40% was recorded with all the catalyst systems. The catalysts used in this work are useful for applications in energy and other value added chemicals.

Key words

Catalysis
Perovskite
Exsolution
Steam reforming
Renewable fuels
Fuel Cell

1.0 Introduction

The global energy demand, environmental concerns and quest for clean energy has placed fuel cell technology at the front because of its simple practicability, energy

[1] Corresponding author: u.ahmed2007@yahoo.com; ahmed.umar@uniabuja.edu.ng
Department of Chemistry, University of Abuja,
Gwagwalada, Abuja, Nigeria.

efficiency, environmentally friendly, fuel flexibility and cost effectiveness [1-4]. The achievements recorded in fuel cell technology have shown that hydrogen driven systems would replace the fast depleting and environmentally reneging fossil-based fuel driven systems in the near future [5-7]. It is believed that the much desired renewable hydrogen feedstock could be obtained through an on-board reforming of hydrogen-rich renewable biomass feedstock [8-11]. Amongst the existing reforming technologies, steam reforming has been found very efficient and quite reliable. At elevated temperatures, biomass decomposition products are steam reformed leading to the formation of gaseous products essentially, H_2, CO_2, CH_4 and CO which could be fed to fuel cell such as solid oxide fuel cells (SOFCs) as renewable fuel to the conventional fossil-based hydrogen [12-14]. Interestingly, unlike Proton-Exchange Membrane (PEM) fuel cell that sees CO as a poison to anode particularly were noble metals are involved and the fuel cell low-temperature operations, the high temperature SOFCs utilizes even CO as a fuel. With the aid a robust catalyst system, the gaseous biomass decomposition products could be made hydrogen and carbon monoxide rich to enhance cell performance and efficiency. One of the obvious resultant problems with the use of such fuel is the degradation of fuel cell performance overtime due to coke deposition and fouling of the catalyst surface or anode material [15-17]. This called for the development of a better catalyst system that can cope with the hash condition that ensured while using such alternative fuel.

Consequently, catalyst material remains central to steam reforming process and many of the existing technologies that are employed in biomass conversion to renewable fuels. Hence, design and development of robust and active catalyst for biomass conversion is attracting much research interest particularly perovskite materials as results of their robust structural and catalytic properties that could be enhanced or improve upon through doping [18,19]. Recently, catalyst design that involves exsolving active metal catalyst from the bulk socketed and decorated on an oxide support is fast gaining prominence as results of its promising catalytic properties and structural doping flexibility [20-21]. In a recent work, Umar, et al (2021) [22] has demonstrated the use of alkaline dopant metals to enhance catalytic and surface properties of exsolved nano-catalyst with perovskite structure for glycerol valorisation. The alkaline modified exsolved catalysts showed not only improved catalytic behaviour but also reduced level of carbon deposition. It was also observed however, that nickel catalyst exsolution was very limited i.e. not

properly enhanced by the alkaline metals attributed to a phenomenon called 'strontium hindrance' as reported in a related work [23,24] with a consequent reduction in the catalyst performance despite their enhanced acidic-basic surfaces. The catalyst performance suggest direct correlation between the extent or level of exsolution and the catalyst-support interaction as well as the overall catalytic activity and ability to suppress fouling of catalyst surface due to carbon deposition. Attempts were made in several related work to enhance the exsolution of metal catalyst through tailoring of reaction and reduction conditions with some promising results [20,21]. With the advances and successes recorded in the development of catalyst system through exsolution phenomenon, suffices to say supported metal catalyst design and chemistry is improved when compared the conventional method of wet impregnation.

Some nickel catalyst systems have shown some great propensity towards decomposition of biomass and hydrocarbon feedstock such as glycerol to gaseous products. However, they get deactivated easily particularly those catalyst systems prepared by wet impregnation as results massive carbon deposition, reoxidation and sintering especially when used or prepared at high temperature [25-29]. Ceria is known to enhance the reducibility of nickel and suppression of fouling of catalyst surface as a result of carbon deposition hence increasing the stability and reusability of nickel catalyst [30]. This was attributed to its enhanced catalyst-support interaction as a result of ceria's redox properties and acid-basic surface which gives it the ability to switch between its oxidation state of Ce^{+4} and Ce^{+3}. Consequently, ceria's versatility in large number of industrial processes and applications has given it economic value that has surpassed many other rare earth metals [31]. Ceria oxides-based catalyst systems are promising catalyst for many applications and were utilised as support and promoter for many catalyst systems such as automotive exhaust catalyst because of its reducibility, redox and oxygen storage-release properties as well as relative stability over varying temperatures [32-35].

Nanostructured ceria particles have been found to demonstrate relatively more impactful catalytic behaviour particularly in reforming of gaseous products for energy and environmental remediation applications [30,31]. Nanostructured nickel catalysts were tailored through the use a modifier Y_2O_3 to stabilise the nickel

catalyst by enhancing catalyst-support interaction in a ZrO_2 supported catalyst system for steam reforming of glycerol in a related work reported by Charisiou et al. 2020 [36]. The addition of the Y_2O_3 into the supported catalyst Ni/ZrO_2 did not only stabilised the catalyst but also improved the oxygen storage capacity of the support and enhanced surface chemistry of the active basic sites as well as surface particle size and population. The structured modification helped to suppress coke deposition with a resultant stabilisation and sustainability of hydrogen yield.

It is also revealed that steam reforming temperature and nature of support influences glycerol conversion and distribution of gaseous products as well as hydrogen yield. The Co-based supported catalysts Co/La_2O_3, Co/AlZnOx and Co/AlLaOx prepared by incipient wetting impregnation have demonstrated high stability and suppression of coking activities attributed to the nature of the support surface chemistry [37]. The Co/AlLaOx catalyst system was found more active, selective and more resistant to coke deposition. In related work, it is established that addition of the right amount of a catalyst modifier such as La_2O_3 to a support in a comparative study between Ni/Al_2O_3 and the modified $Ni/La\text{-}Al_2O_3$ enhances catalyst-support interaction, active site strength, concentration and distribution with a consequent improved catalytic activity and stability [38]. The type and nature of the carbon deposited was also influenced by the modifier. While the $Ni/La\text{-}Al_2O_3$ catalyst was associated with amorphous carbon deposited on the support that allows easy regeneration and reusability of the catalyst, Ni/Al_2O_3 was associated with more severe graphitic carbon deposited on the active sites. Despite the preference on the use of cheap transition and rare earth metals in the design and development of metal catalysts for steam reforming of glycerol, expensive and precious metals have also shown some promising results particularly at low reforming temperature as reported by Silva et al. 2019 [39]. However, catalyst deactivation due to rapid formation of carbon containing liquid products and deposition of amorphous carbon was observed within few hours of the test though oxidative regeneration and removal of the easy-to-remove amorphous coke has helped to enhance the catalyst reusability.

The innovative catalyst design and synthetic method of exsolution [40,41] that allows control over general morphology such as particle size and distribution and doping flexibility has opened possibilities for tailoring and fine tuning structural

properties for diversified morphological architecture in order to achieve the much desired robust catalyst systems for different applications [41-45]. In this work the influences of A-site dopant metal (ceria) and lattice defect on the exsolution of catalyst nanoparticles in the B-site of perovskite and catalytic behaviour of the systems in relation to steam reforming of glycerol is reported. Particularly, ceria was selected to demonstrate its influences and mediation in the exsolution process and compared to some metal such as alkaline metals. The aim was to generate syngas as well as hydrogen gas from the low cost, readily available and renewable glycerol from biodiesel synthesis as alternative, renewable fuel for the utilization of solid oxide fuel cells and for production of other value-added chemicals. It is also believed that catalytic conversion of CO_2 and CH_4 (major contributors to greenhouse effect) to CO and H_2 (syngas) through dry reforming and steam reforming will limit their environmental effects (global warming). Series of ceria containing non-stoichiometric titanate perovskite catalyst systems were designed and tailored to be A-site deficient to mediate and facilitate the exsolution of the B-site nickel catalyst, enhance basic properties, catalyst-support interaction and other catalytic behaviour as well as suppression of carbon deposition. Possible formation of alloyed catalyst systems between the exsolved metals (Ni, Fe, Co) and innovative synergic effect on the catalytic behaviour in relation to steam of glycerol was also investigated. It is also to demonstrate the structural stability and exsolution of nano catalyst, selectivity for the desired products and ability to suppress catalyst deactivation as a results of carbon deposition that is associated with overstretched highly oxygen deficient perovskite catalyst with A-site deficiency of 2.5% in one of the formulations as against the known tolerable A-site deficiency and doping limit of 2% of $SrTiO_3$ type perovskite.

2.0 Materials and Methods

2.1 Catalyst synthesis and processing

The catalysts were prepared using modified solid state synthesis as described by Umar et al (2021) [22]. In this method, required weight of dried oxides of metals and carbonates was dried at elevated temperatures of 300-800 ^oC were measured while hot (at 300 ^oC) and mixed in a beaker along with the required weight of nitrate of some metals as specified in the catalyst formulation. Hypermer KD-1(polyester/polyamide copolymer) dispersant was added to the mixture to improve dispersion and suppress agglomeration. Acetone was added to the mixture and

homogenised using ultrasonic probe and eventually dried on hot plate then calcination at 1000 ^{o}C. Further calcination was carried out at 1400-1430 ^{o}C to obtain the ready-made or as-prepared/pre-reacted samples of the catalyst systems. To obtain the exsolved nano catalysts, the ready-made catalysts were subjected to reduction process at 900 ^{o}C in tubular furnace for 30 hours under 5% H_2/Ar mixture.

2.2 Catalyst Characterization

Room temperature crystallographic data were collected on Pan-Analytical Empyrean X-Ray Diffractormeter (XRD) operating on reflection mode using Cu-Kα_1 radiation at λ = 1.5406 Å and 10-90 2θ angle range for 1 hour.

Surface area, pore volume and size determination were carried out by Brunauer-Emmitt-Teller (BET) and Barrette-Joyner-Halenda (BJH) methods respectively using nitrogen adsorption/desorption at 77.35K using Micrometrics TriStar II 3020 model. Before the analysis, samples were heated for 3 hours at 120 ^{o}C to remove moisture and other residual gases.

Morphology and surface properties of the catalyst were investigated using Field Emission Scanning Electron Microscopy (FESEM) JEOL JSM6700F.

Thermo-gravimetric Analysis using NETZSCH TG 209 analyser was used to investigate reducibility and thermal stability of the materials. Each sample was run in air/argon mixture to 900 ^{o}C at heating rate of 3^{o}/min in aluminium crucible, after cooling, the sample was then run in reducing environment using 5%H_2/Argon mixture to same temperature.

Coking activities resulting to carbon depsition from the catalysis process on the used catalyst surface was characterized using temperature pogrammed oxidation (TPO) on NETZSCH STA 449C trigravimetric analyser equiped with thermostar mass spetrometer. Specific weight of the spent catalyst was taken into the thermogravimetric analyser and argon gas was used to flush the system residual gases in the system. Surface carbon was oxidised to CO_2 using O_2 to temperatures of 900 ^{o}C. Gases produced were trapped and chanelled for anaysis using were mass spectrometer.

2.3 Catalytic gasification and steam reforming testing

A fixed bed in a quartz tube reactor (8 mm internal diameter (ID), 10mm outer diameter (OD) and 24cm long) was used for run steam reforming catalysis of pure glycerol at 700 ^{o}C and atmospheric pressure. The schematic diagram of the reactor assembly and details of the procedure is as shown and described in Umar, et al (2021) [22].

3.0 Results and Discussion

3.1 Catalyst Characterization

3.1.1 CRYSTALLOGRAPHIC DATA AND ANALYSIS

The room temperature X-ray Diffraction pattern of the materials shown in Figure 1 was collected and used to characterize the phase purity of the synthesised catalyst materials; $La_{0.7}Ce_{0.1}Fe_{0.3}Ni_{0.1}Ti_{0.6}O_{3-\delta}$(LCeFNT), $La_{0.8}Ce_{0.1}Ni_{0.4}Ti_{0.6}O_{3-\delta}$(LCeNT), $La_{0.6}Ce_{0.05}Sr_{0.1}Ni_{0.1}Ti_{0.9}O_{3-\delta}$(LCeSrNT) and $La_{0.7}Ce_{0.1}Co_{0.3}Ni_{0.1}Ti_{0.6}O_{3-\delta}$(LCeCoNT) respectively. The A-site deficient materials were designed to have different vacancies and dopant materials for comparison. Analysis by Indexing of the XRD pattern as shown in Figure 1a and b confirms that all the reflections or peaks in the pattern peaks or are typical of perovskite structure [42,46] suggesting successful synthesis of pure and single phase perovskite materials except $La_{0.7}Ce_{0.1}Fe_{0.3}Ni_{0.1}Ti_{0.6}O_{3-\delta}$ which showed some anomalous behaviour as explained below.

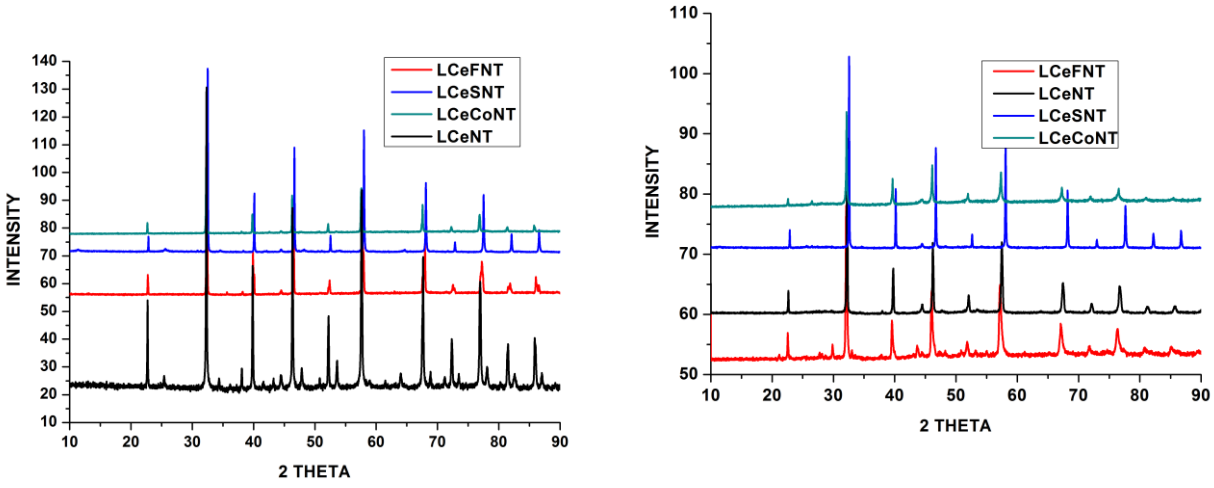

Figure 1: The XRD patterns of the synthesized A-site deficient nickel-based titanate perovskites of the samples showing their phase purity **a,** for the as prepared samples prior to reduction and **b,** the reduced samples showing them maintain their perovskite structure with no evidence of decomposition or disintegration after reduction for 30 hours at 900 ^{o}C in hydrogen.

It is interesting to note that the $La_{0.6}Ce_{0.05}Sr_{0.1}Ni_{0.1}Ti_{0.9}O_{3-\delta}$ perovskite with 25% (α=0.25) A-site deficiency was also successfully synthesized. There is no evidence of formation of new or extra phase in the XRD patterns. This new material particularly has demonstrated a robust exsolution of nickel nanoparticles well distributed on its surface as seen in Figure 5. Rietveld refinement of the XRD patterns of the materials before reduction revealed different symmetry and space groups for the as-prepared materials as shown in Table 1.

The overlaid patterns shows a slight shift in the 2θ position revealing the influence of the differences in ionic size among the dopant ions used and changes associated with structural symmetries shown by the samples in the refinement data of Table 1. The stability of the reduced samples in hydrogen atmosphere and maintenance of their perovskite structure after prolong reduction for 30 hours at 900 ^{o}C is also supported by the XRD patterns of Figure 1b when compared to other materials that decomposes in reducing atmosphere at elevated temperatures [47,48]. This is further corroborated by the thermogravimetric analysis shown in Figure 4. There is also evidence of reduction in the intensity of the perovskite peaks or complete disappearance after reduction when compared to that of the original sample XRD pattern before reduction and the splitting pattern of the peaks is also noticeably less. This observation becomes more apparent in $La_{0.8}Ce_{0.1}Ni_{0.4}Ti_{0.6}O_{3-\delta}$ perovskite which shows fewer peaks in Figure 1b compared to the more seen on the XRD pattern of Figure 1a above before reduction which suggests evolution to higher symmetry by the reduced materials. There increase in d-spacing as suggested by shift to smaller 2θ angles also resulting from increase in volume of the unit cell caused by the redox behaviour of titania's transformation from smaller Ti^{4+} ions to larger Ti^{3+} during electronic transfer influence by reducing atmosphere.

Table 1: Summary of the refinement data

Catalyst	Abbreviation	Space group	Cell Parameter	Cell Volume	Refinement fit parameter
$La_{0.8}Ce_{0.1}Ni_{0.4}Ti_{0.6}O_{3-\delta}$	LCeNT	*P b n m*	a= 5.5452 b= 5.5329 c= 7.8221	239.992	R_p=6.82, R_{wp}= 9.54, R_{Exp}=12.14, X^2=0.619
$La_{0.6}Ce_{0.05}Sr_{0.1}Ni_{0.1}Ti_{0.9}O_{3-\delta}$	LCeSrNT	*I 4 / m c m*	a= 5.5025 b= 5.5025 c= 7.7820	235.622	R_p=10.2, R_{wp}= 13.8, R_{Exp}=7.92, X^2=3.05
$La_{0.7}Ce_{0.1}Co_{0.3}Ni_{0.1}Ti_{0.6}O_{3-\delta}$	LCeCoNT	*I 2/a*	a= 7.8459 b= 5.5408 c= 5.4007	240.543	R_p=7.24, R_{wp}= 9.54, R_{Exp}=8.54, X^2=1.25
$La_{0.7}Ce_{0.1}Fe_{0.3}Ni_{0.1}Ti_{0.6}O_{3-\delta}$	LCeFNT	-	-	-	-

The Rietveld refinement data in Table 1 shows that space group, lattice parameter 'a' and the cell volume varies among the perovskite materials synthesised in this work reflecting the different dopant and level of defect due to A-site deficiency. The original patterns have shown good matching and correlation with the refinement crystal model and the proposed space groups as seen in Figure 2a-c. The crystal model also shows the orientation of the atoms in space and octahedral distortions i.e. in-out-of-phase tilting in the same Figure 2a-c. It is interesting to note that despite all the samples contains ceria, they all exhibited different symmetry and distortions which is clear manifestation of the influence of the varying other dopants used and A-site deficiency amongst the catalyst systems. The space group and structural model suggests distortions along all the crystallographic axes and seen Figure 2a-c.

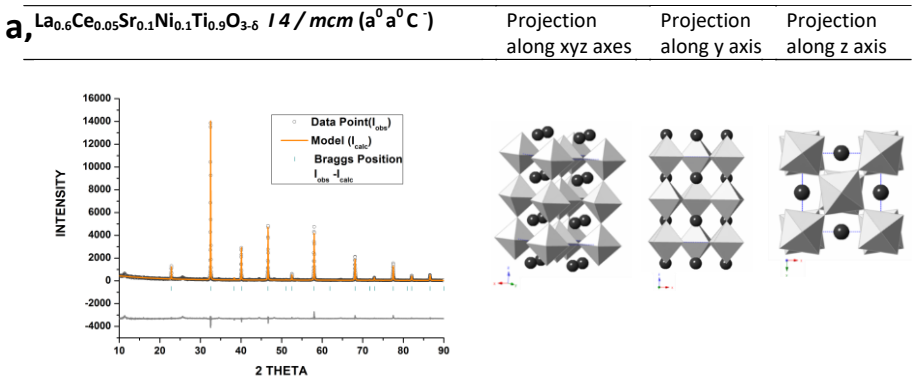

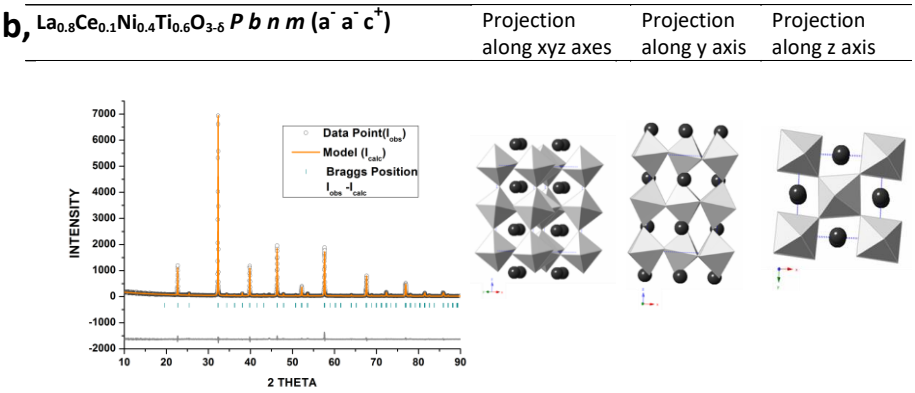

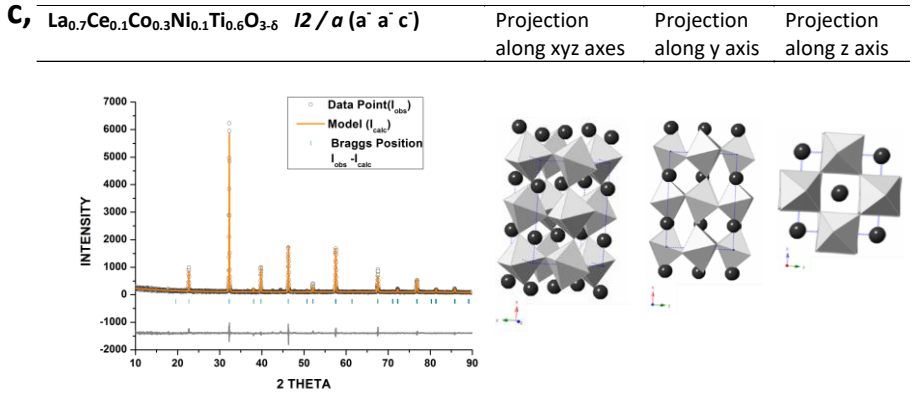

Figure 2: The proposed tetragonal model matching with the XRD pattern of the synthesised materials and the projection of the structure showing out-of-phase tilting along z=axis as the *I4/mcm* space group suggest in **a,** $La_{0.6}Ce_{0.05}Sr_{0.1}Ni_{0.1}Ti_{0.9}O_{3-\delta}$ and out-of-phase tilting along x and y axis but in-phase tilting along x axis as the p b nm space group suggest in **b,** $La_{0.8}Ce_{0.1}Ni_{0.4}Ti_{0.6}O_{3-\delta}$ and **c,** $La_{0.7}Ce_{0.1}Co_{0.3}Ni_{0.1}Ti_{0.6}O_{3-\delta}$ shows out-of-phase tilting along all the axes axis as the *I2/a* space group suggests.

The refinement process administered on the $La_{0.7}Ce_{0.1}Fe_{0.3}Ni_{0.1}Ti_{0.6}O_{3-\delta}$ sample was not complete or successful as a result of the apparent complexity associated with its structure. Many attempts were made and the entire space groups proposed could not match or fit it accurately. The peaks splitting pattern observed for this particular material is not known to perovskite structure as exemplified in Figure 3. These uncommon splitting pattern of $La_{0.7}Ce_{0.1}Fe_{0.3}Ni_{0.1}Ti_{0.6}O_{3-\delta}$ sample peaks was traced to a possible formation of two perovskites supper imposed in one another and hence could not fit or match a specific structural model used for it.

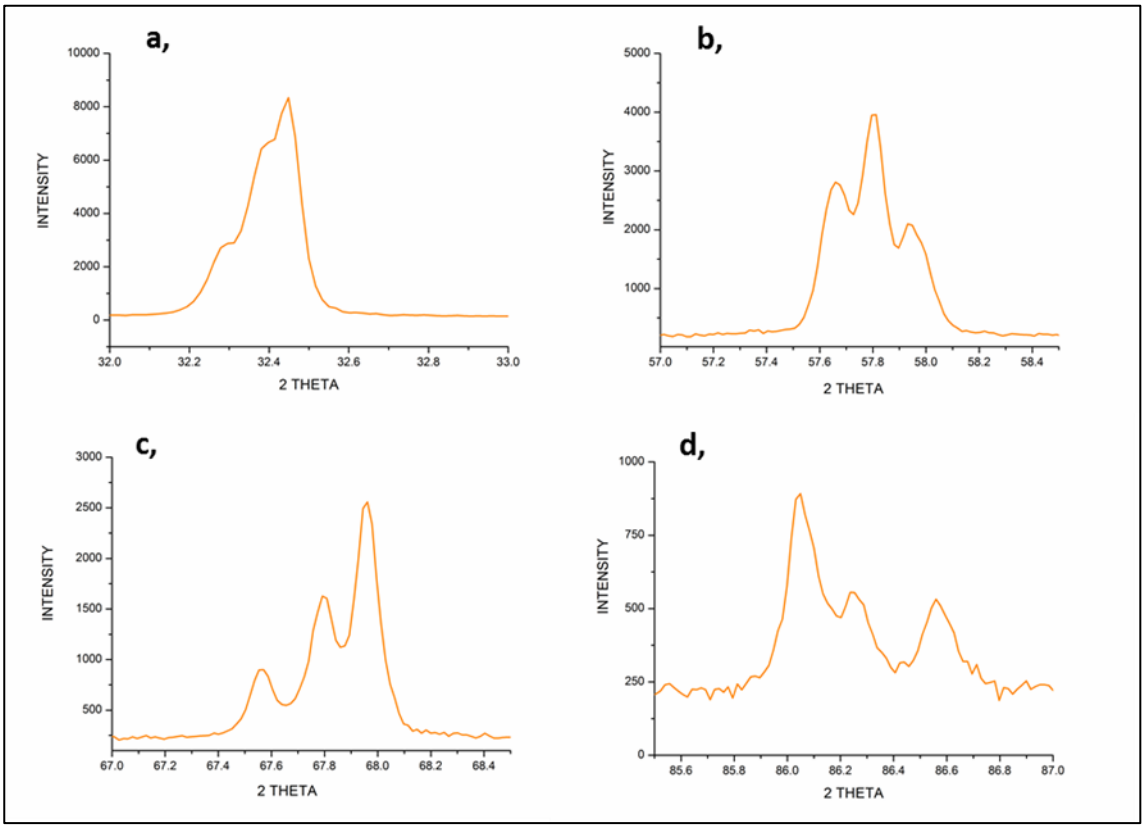

Figure 3 Is showing the multiple splitting pattern of peaks from the $La_{0.7}Ce_{0.1}Fe_{0.3}Ni_{0.1}Ti_{0.6}O_{3\pm\delta}$ catalyst XRD. The peaks corresponds to the following hkl values **a,** 220 **b,** 422 **c,** 440 and **d,** 444 respectively.

3.1.2 STABILITY OF THE NICKEL-BASED A-SITE DEFICIENT SAMPLES BY THERMO-GRAVIMETRIC INVESTIGATION IN AIR AND HYDROGEN

Thermal stability and stability of the materials in air and hydrogen atmosphere was investigated via thermo-gravimetric method of analysis and the results obtained are as shown in Figure 4a and b. The Figure 4a shows the TGA profile of the as prepared samples. The TGA profile as denoted by the segmented dotted line shows oxidation in air and reduction in hydrogen atmosphere respectively. In Figure 4a, all the materials have shown consistent and persistent thermal stability in air atmosphere at all temperatures under study hence showed no evidence of weight loss or gain. In the reduction process as shown in the second segment of Figure 4a, weight loss of about 1.36% (0.5 mg) in the hydrogen atmosphere was observed for $La_{0.7}Ce_{0.1}Fe_{0.3}Ni_{0.1}Ti_{0.6}O_{3-\delta}$ catalyst. There is also a slight weight loss due to $La_{0.6}Ce_{0.05}Sr_{0.1}Ni_{0.1}Ti_{0.9}O_{3-\delta}$ with 2.5% A-site deficiency and a little corresponding weight loss of about 0.7% (0.29 mg) from $La_{0.7}Ce_{0.1}Co_{0.3}Ni_{0.1}Ti_{0.6}O_{3-\delta}$ containing Co. The XRD pattern of these compounds in Figure 1b showed no evidence of decomposition of these materials or segregation in the hydrogen atmosphere hence these weight losses are partly attributable to the oxygen storage-release properties of ceria.

Figure 4b shows the TGA profile of the reduced samples in air and hydrogen respectively as also shown by the dotted line of Figure 4b. There is a weight gain by the ceria-containing samples in air which is attributable to gain of oxygen by the highly reduced samples. Similar trend of weight loss due to oxygen loss during reduction is evident in the second segment of the TGA profile. Essentially, $La_{0.7}Ce_{0.1}Fe_{0.3}Ni_{0.1}Ti_{0.6}O_{3-\delta}$ profile stood out distinctively in both segments showing a large weight gain of about 2.87% (1.33 mg) and 2.01% (0.72 mg) weight loss. $La_{0.7}Ce_{0.1}Co_{0.3}Ni_{0.1}Ti_{0.6}O_{3-\delta}$ also showed similar trend, recording a weight loss of 1.39% (0.64 mg) and gain of 2.60 % (1.19 mg). The ceria's oxygen storage-release properties might be partly responsible and the additional contribution due to the redox active Fe in $La_{0.7}Ce_{0.1}Fe_{0.3}Ni_{0.1}Ti_{0.6}O_{3-\delta}$ gave that compound an edge over the rest materials.

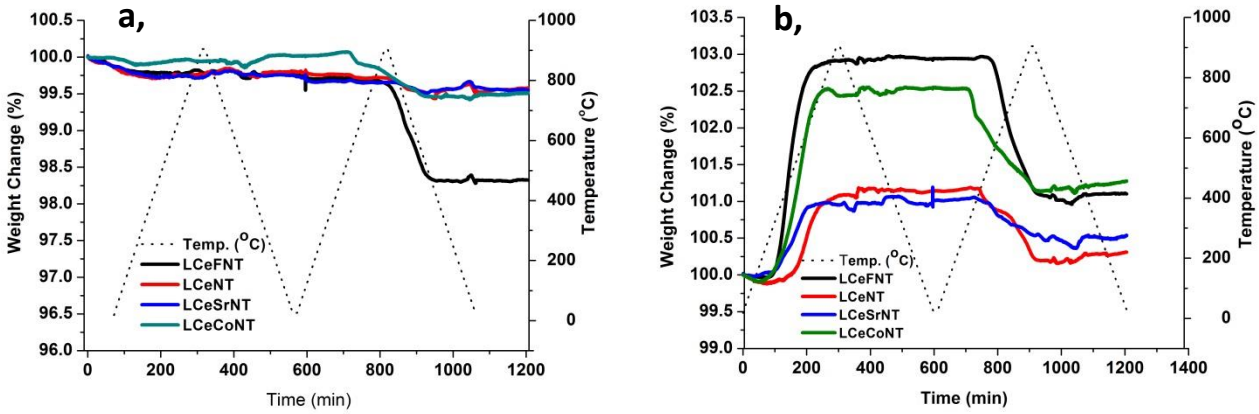

Figure 4: Thermo-gravimetric analysis showing stability of the samples in both air and hydrogen atmosphere heated to 900°C at heating rate of 3°/min **a,** TGA of the as-prepared samples before exsolution by reduction. The first segment of the denoted line shows oxidation in air and the second segment of the dotted line shows reduction in hydrogen **b,** TGA of the reduced samples after exsolution. The first doted segment shows oxidation of the samples in air and the second reduction in hydrogen atmospheres respectively.

To strengthen this observation further, the TGA profile $La_{0.6}Ce_{0.05}Sr_{0.1}Ni_{0.1}Ti_{0.9}O_{3-\delta}$ doped with only 5% ceria when compared to the 10% in others yielded the lowest weight loses though its highest titania content that is so redox inactive would have influenced the observed trend. It is evident from the XRD pattern of the reduced samples as explained above; these weight changes are attributable to oxygen storage-release properties of ceria and not segregation or decomposition of these samples [49]. These observations support the thermal stability and structural integrity of these perovskite materials in air and hydrogen. Furthermore, suffices to observe that integration of other dopant metals in these formulations have strengthened the thermal and structural stability of ceria to high temperature operations [30, 31,47]. Consequently, tailoring oxygen storage-release property of perovskite material could help to improve oxygen ion mobility and catalytic properties for enhanced oxidation of gassified biomass decomposition of products particularly carbonaceous species that could deactivate catalyst surfaces and facilitate product dissemination.

3.1.3 PHYSICOCHEMICAL PROPERTIES

Surface area, pore size and volumes of the solid state synthesized nickel-based titanates were investigated and results of the analysis are shown in Table 2. High temperature solid state reaction temperatures of 1430 °C was used for the synthesis and reduced in 5%H_2 at 900 °C for 30 hours in a tube furnace. The

results show an increase in the surface area of the materials after reduction. The surface exsolution has transformed surface general morphology as seen in the SEM micrographs in Figure 5 with catalyst particles uniformly distributed on the surface instead of getting imbedded in the bulk leading to the observed increase in surface area. Perovskite materials naturally exhibit naturally poor surface area because they are conventional synthesized at higher temperatures (800-1500 ^{o}C) [50,51] and the results in this work suggest exsolution as a method of synthesis could be used to enhance the poor surface area of perovskite materials [20,52], and the results is favourably comparable to the use of templating agents [53,54]. The reduction process resulted in nickel particles and other dopants (Fe and Co and their alloy) exposed to the surface and dispersed uniformly across the surface as a result of exsolution with consequent increase in surface area for robust catalytic behaviour.

Table 2: Physicochemical Properties

Catalyst Systems	A-Site deficiency	Surface Area before Reduction (m^2/g)	Surface Area After Reduction (m^2/g)
$La_{0.7}Ce_{0.1}Fe_{0.3}Ni_{0.1}Ti_{0.6}O_{3-\delta}$	20	3.88	5.65
$La_{0.8}Ce_{0.1}Ni_{0.4}Ti_{0.6}O_{3-\delta}$	10	2.37	3.81
$La_{0.6}Ce_{0.05}Sr_{0.1}Ni_{0.1}Ti_{0.9}O_{3-\delta}$	25	2.21	3.91
$La_{0.7}Ce_{0.1}Co_{0.3}Ni_{0.1}Ti_{0.6}O_{3-\delta}$	20	2.27	4.82

Generally, though the surface area is not large enough and that there is no consistent or conclusive correlation between the surface area observed among the materials and the defect due to A-site deficiency, it is observable that materials have shown improved surface area and robust active sites that could enhance catalytic activity when compared to other perovskite catalyst systems that are not exsolved.

3.1.4 MICROSTRUCTURE OF THE EXSOLVED NANO CATALYSTS

The SEM micrograph of the exsolved nanoparticle of the catalysts as shown in Figure 5a-f revealed transformation of the surface morphology covered by well distributed oxide-supported metal nanoparticles grown from the host perovskite structure. The dotted and dispersed particles are largely nickel nanoparticles, some Fe, Co or Ni-Fe and Ni-Co alloys resulting from the exsolution phenomenon arising from the migration of oxygen ion in the bulk to the surface due to imbalance that removal of surface oxygen during the reduction process have created.

Consequently, to balance such non-stoichiometry and instability, expulsion of metals occurs from the non-defective B-site onto the surface anchored and supported on the titania oxide [41]. It is evident in the micrograph images that the expelled nanoparticle catalysts are largely anchored and socketed on the outer surface of the materials rather than in the bulk. These transformations have exposed the active sites to the surface for more effective catalysis process and have also naturally improved catalyst-support interaction and enhanced reducibility of nickel catalyst [22,23].

The SEM micrograph in Figure 5a-g shows that individual formulation responds differently to the reduction process and the exsolution. The ceria containing materials (Figure 5a-d) shows a good exsolution when compared to non-ceria containing material (Figure 5e-g). This shows that choice of dopant metal on the A-site of the perovskite material could be tailored to enhance migration of metal catalyst from the B-site onto the surface (exsolution) to enhance structural and catalytic properties. Although the behaviour of the material is attributed to the constituent dopant or metal, the defect due to A-site deficiency has played an important role. For instance, comparing $La_{0.4}Sr_{0.2}Ca_{0.3}Ni_{0.1}Ti_{0.9}O_{3-\delta}$ (Figure 5**f**) and $La_{0.6}Ce_{0.05}Sr_{0.1}Ni_{0.1}Ti_{0.9}O_{3-\delta}$ (Figure 5**c**), it is evident the replacement of calcium with ceria has suppressed the so-called ‘Sr hindrance’ believed to hinder exsolution of Ni in $La_{0.4}Sr_{0.2}Ca_{0.3}Ni_{0.1}Ti_{0.9}O_{3-\delta}$ and also reported in a related work by Neagu et al., (2015) [23] and Umar et al., (2021) [22]. Similarly, the combined influences of defect due to A-site deficiency and choice of dopant metals clearly manifests when comparing $La_{0.7}Ce_{0.1}Fe_{0.3}Ni_{0.1}Ti_{0.6}O_{3-\delta}$ (Figure 5**b**) and $La_{0.5}Sr_{0.4}Fe_{0.1}Ni_{0.1}Ti_{0.8}O_{3-\delta}$ (Figure 5**e**). Furthermore the $La_{0.6}Ce_{0.05}Sr_{0.1}Ni_{0.1}Ti_{0.9}O_{3-\delta}$ catalyst system with 25% A-site deficiency was better excluded than $La_{0.4}Sr_{0.2}Ca_{0.3}Ni_{0.1}Ti_{0.9}O_{3-\delta}$ and $La_{0.8}Ca_{0.1}Cr_{0.2}Ni_{0.2}Ti_{0.6}O_{3\pm\delta}$ with only 10% A-site deficiency. In addition to introducing ceria, increasing deficiency and defect also increases ion mobility within the systems [55,56]. More so, all the four samples containing ceria (a, b, c and d) have demonstrated better exsolution and uniform dispersion of B-site cations compared to non-ceria containing materials (e, f and g) that showed limited exsolution of nanoparticles.

Interestingly, the new material $La_{0.6}Ce_{0.05}Sr_{0.1}Ni_{0.1}Ti_{0.9}O_{3-\delta}$ (Figure 4**c**) with the 25% A-site deficiency, apart from exhibiting excellent exsolution behaviour with nickel

nanoparticles dispersed uniformly on its surface, the TGA analysis of the sample before and after reduction as seen in Figure 3 has confirmed the relative redox stability of this sample as no evidence of possible decomposition or segregation was noticed on the TGA profile. The observation is corroborated by the XRD pattern of the sample after reduction as seen in Figure 1 above. This is against the consequent decomposition or segregation of the constituent atom that happens when the limit of deficiency or excess is exceeded. This goes to show that the deficiency or excess could be stretched with no apparent damage to the structural integrity or stability of the sample provided the right constituent dopants tolerant of that situation are selected and used in a suitable ratio. Consequently, tailoring A-site deficiency and choice of constituent dopant metal could help in catalyst design to significantly transform surface morphology such as exsolution and distribution of nanoparticle metal catalysts for improved for enhanced and robust catalytic activity or behaviour.

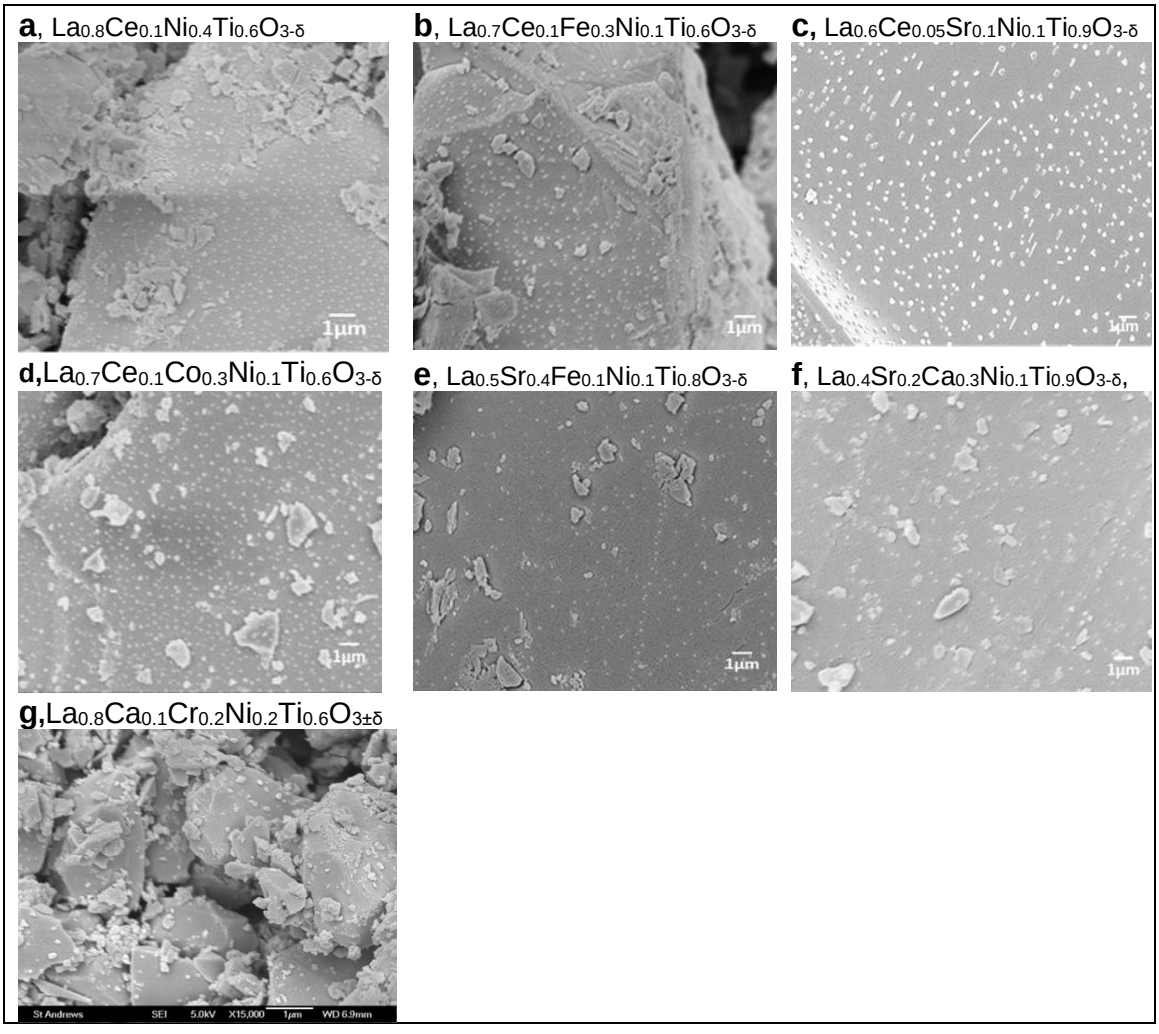

Figure 5 Micrograph of the A-site deficient titanates showing exsolved metal particles in

a, $La_{0.8}Ce_{0.1}Ni_{0.4}Ti_{0.6}O_{3-\delta}$, **b**, $La_{0.7}Ce_{0.1}Fe_{0.3}Ni_{0.1}Ti_{0.6}O_{3-\delta}$, **c,** $La_{0.6}Ce_{0.05}Sr_{0.1}Ni_{0.1}Ti_{0.9}O_{3-\delta}$ **d,** $La_{0.7}Ce_{0.1}Co_{0.3}Ni_{0.1}Ti_{0.6}O_{3-\delta}$, **e,** $La_{0.5}Sr_{0.4}Fe_{0.1}Ni_{0.1}Ti_{0.8}O_{3-\delta}$, **f,** $La_{0.4}Sr_{0.2}Ca_{0.3}Ni_{0.1}Ti_{0.9}O_{3-\delta}$ and **,g** $La_{0.8}Ca_{0.1}Cr_{0.2}Ni_{0.2}Ti_{0.6}O_{3\pm\delta}$

3.2 Catalytic activity and selectivity of the materials for the gaseous products

To evaluate the catalyst behaviour and activity, catalytic test was carried out at 700 ^{o}C using pure glycerol at atmospheric pressure and steam-to-carbon ratio of 1:3 on 50mg catalyst amount. 2.60 x 10^{-4} mole/min molar flow rate of glycerol-water solution and WHSV of 28 h^{-1} was maintained throughout the duration of the test. The aim was to generate stream of syngas or hydrogen gas for utilization in solid oxide fuel cell as alternative renewable fuel to the conventional fossil-based hydrogen or production of other value added chemicals. The results of the test as presented in Figure 6a shows catalytic activity in terms of stream of gases generated in mole/mole of glycerol against hydrogen selectivity.

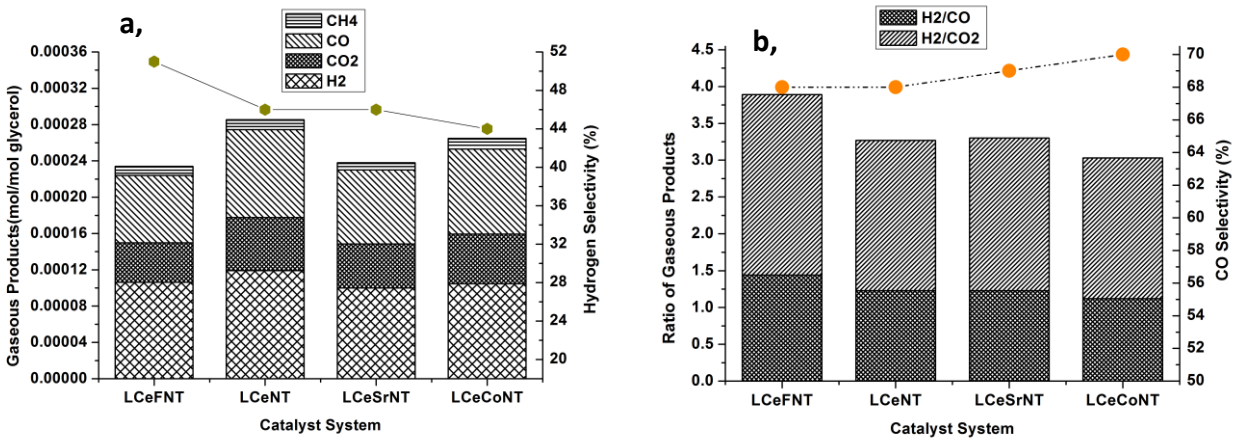

Figure 6**a**, Catalyst performance evaluation showing catalytic activity as gaseous products produced in mol/mol in comparison with hydrogen selectivity. **b**, Ratio of the gaseous product in relation to CO selectivity

The steam reforming results show that the catalyst systems are active and selective to the gaseous species H_2, CO_2, CO and CH_4 detected during the analysis with H_2 and CO appearing as are the predominant gases produced with all the catalyst systems. The H_2/CO_2, H_2/CO ratios and high CO selectivity relatively of Figure 6b as well as high hydrogen selectivity in Figure 6a all attests to these observations. The analysis in Figure 6b show a high value of H_2/CO_2 than H_2/CO which suggests more CO was produced than CO_2. This is attributable to the catalyst effective gasification and oxidation of the glycerol decomposition carbonaceous products via

reactions such as reverse water gas shift reaction (RWGSR) and glycerol rapid pyrolysis due to kinetics and nickel contents as exemplified in the equations provided below.

$C_3H_8O_3 \rightarrow 3CO + 4H_2$ $\Delta H = +251$ kJ mol^{-1} at 298k Eqn1

$CO + H_2O \leftrightarrow CO_2 + H_2$ $\Delta H = -41$ kJ mol^{-1} at 298k Eqn2

$C + H_2O \leftrightarrow CO + H_2$ $\Delta H = +131$ kJmol^{-1} at 298k Eqn3

$C + CO_2 \leftrightarrow 2CO$ $\Delta H = -172$ kJmol^{-1} at 298k Eqn4

The catalyst performance is corroborated by the excellent suppression of carbon deposition reported in Figure 8. Another important contributor to large production of H_2 and CO is the combination of dry reforming of methane (DRM) and steam reforming of methane (SRM) reactions catalysed by the catalysts used in this test.

$CH_4 + CO_2 \leftrightarrow 2H_2 + 2CO$ $\Delta H = +247$kJmol^{-1} at 298k Eqn5

$CH_4 + H_2O \leftrightarrow 3H_2 + CO$ $\Delta H = +206$kJmol^{-1} at 298k Eqn6

Figure 5a shows a limited production of CH_4 and CO_2 which suggests the catalyst systems actively catalysed these reactions to produce large syngas with robust suppression of carbon deposition as supported by the analysis in Figure 8. These results and observations enhances industrial applicability of DRM with these catalyst systems since carbon deposition and sintering were identified as the major problems associated with the use of DRM in practical industrial applications [31]. The large synthesis gas produced could be utilised not only in fuel cell technology but also in production of other value-added chemicals and in Fischer-Tropsch process for the production of long-chain hydrocarbons and oxygenate renewable chemicals [30,31]. The test result also shows that the catalyst could be used to remove or reduce the concentration CH_4 and CO_2 as main agents of global warming from the environment via DRM and SRM. Considering the amount of catalyst used (50mg) in this test, the catalyst samples gave a reasonable conversion to gaseous products with a good selectivity for H_2 and CO comparable to other reported work [16,31], despite limiting factors such as water gas shift reaction, formation of acrolein and carbonyl compounds and too much through put due to small catalyst bed that might have influenced the desired products yield.

From the test so far carried out in this work, one cannot correlate defect due to A-site deficiency to the observed performance conclusively. However, it is observable that the high CO selectivity >60% and H_2 selectivity >40% recorded virtually with all

the samples could be attributed to enhanced oxidation of the carbon containing residues by the catalyst due to good oxygen mobility in them as results of their A-site deficiency defect as well as oxygen storage-release properties of the dopant ceria[43,45]. The basic-acidic properties of ceria and alkaline dopants used in some is also an important parameter [22, 30,32]. Therefore defect chemistry due to A-site deficiency and choice of doping metals for both A-site and B-site could be tailored to improve B-site metal catalyst exsolution for biomass conversion to renewable hydrogen and syngas.

It is important to observe that surface area of the ceramic materials influences the concentration or amount of exsolved nano catalyst and has contributed to the observed catalytic activity or behaviour of the catalyst systems. The trend of catalytic activity in relation to generation and distribution of stream gaseous products as shown in Figure 6a is a clear manifestation of the trend of surface area of both the ceramic materials before reduction and the exsolved matrials after reduction as seen in Table 2. Catalysis been a surface phenomenon is influenced by the surface area of perovskite ceramics. The results of the catalysts test have demonstrated that the amount of exsolved catalysts is related to the surface area of the original perovskite material and so also catalytic activity.

3.3 Stability of the catalyst systems to prolong usage against deactivation

The catalysts systems were subjected to long hours of testing to further analyse their activity and stability to agents of deactivation such as carbon deposition, sintering and catalyst poisoning due to prolonged usage in gaseous stream. The performance was investigated by monitoring hydrogen production per mole of glycerol over time for 10 hours. The test was carried out using continuous flow of pure glycerol-water mixture at 700 ^{o}C and steam-to-carbon ratio of 3:1 at atmospheric pressure. WHSV of 28 h^{-1} was maintained throughout the duration of the test and result obtained is as shown in Figure 7. The catalyst systems have shown consistent production of hydrogen with no evidence of much loss of activity. This observation suggests remarkable resistance to catalyst deactivation as no evidence of much or serious loss of performance was recorded. The $La_{0.8}Ce_{0.1}Ni_{0.4}Ti_{0.6}O_{3-\delta}$ despite its initial good performance, the hydrogen yield reduced rapidly within two hours of the test before stabilizing. Both $La_{0.7}Ce_{0.1}Fe_{0.3}Ni_{0.1}Ti_{0.6}O_{3-\delta}$ and $La_{0.6}Ce_{0.05}Sr_{0.1}Ni_{0.1}Ti_{0.9}O_{3-\delta}$ showed similar trend. The drop in hydrogen production is attributed to the intense catalytic activity they

attracted to their surfaces. Nonetheless, the stability of the $La_{0.6}Ce_{0.05}Sr_{0.1}Ni_{0.1}Ti_{0.9}O_{3-\delta}$ catalyst with the overstretched A-site deficiency of 25% is remarkable.

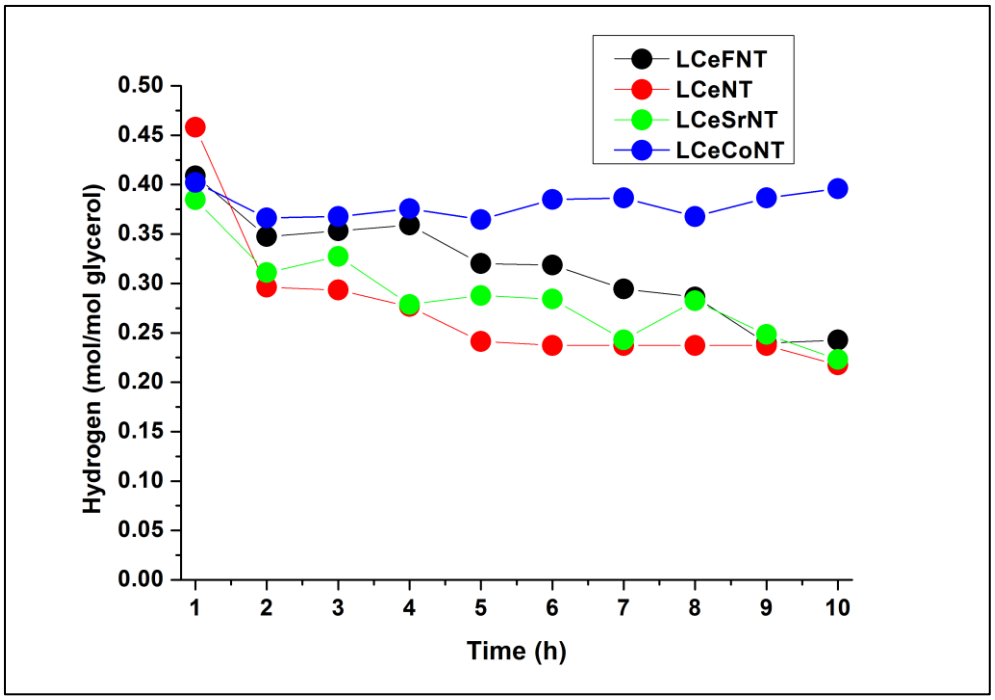

Figure 7 Comparing catalytic activity and stability of the catalysts by monitoring how hydrogen production (mol/mol of glycerol) changes over time for ten hours.

Generally, the catalytic activity and hydrogen production seems more stable with $La_{0.7}Ce_{0.1}Co_{0.3}Ni_{0.1}Ti_{0.6}O_{3-\delta}$ and $La_{0.7}Ce_{0.1}Fe_{0.3}Ni_{0.1}Ti_{0.6}O_{3-\delta}$ catalyst systems over time. The sustained performance attest to the robust properties of the catalyst systems particularly their A-site deficiency and oxygen storage-release properties of ceria which are known to enhance oxygen ion mobility that facilitated the effective oxidation of carbonaceous decomposition products from glycerol pyrolysis and consequently hindered catalyst deactivation by coking activity or poisoning. This compares with work reported by Neagu et al, (2015) [23] and Papaioannou et al (2019) [24]. The relatively enhanced performance of $La_{0.7}Ce_{0.1}Co_{0.3}Ni_{0.1}Ti_{0.6}O_{3-\delta}$ and $La_{0.7}Ce_{0.1}Fe_{0.3}Ni_{0.1}Ti_{0.6}O_{3-\delta}$ is also as results of the synergic contribution of the metal dopants in the alloy of Fe-Ni and Co-Ni active sites exsolved on the catalysts surface which tends to be more active than a single metal sites [24,57,58]. Hence, the disparity in their performance could be traced to not only extent of defect in them but also their difference in the chemical constituents. Consequently, suffice it to say defect chemistry and constituent metals or dopants could play an important

role in tailoring perovskite structures for better catalytic behaviour and should be explored in designing robust catalyst systems.

3.4 Control of carbon deposition activities

The resistant of the catalyst systems to carbon deposition on their surfaces during catalytic activity was investigated to further support their robust properties. Prolong usage of the catalyst exposes their surfaces to lots of carbonaceous residues of different structures and types from the biomass decomposition products that block active sites, pores and consequent deactivation of catalyst thereby limiting the life span and reusability of the catalyst [59-61]. The spent catalyst systems after ten hours of steam reforming of glycerol was subjected to temperature programmed oxidation in oxygen atmosphere and reaction condition stated in section 1.2.2. above. During temperature programmed oxidation, all the carbon deposited on the catalyst surface was converted to CO_2 by oxidation and characterised by identifying their type and location as well as level or extent of coking. The TGA profile in Figure 8 represents the extent or level of carbon deposition whilst the CO_2 peaks suggests the temperature at which bulk of the carbon oxidised to CO_2 which depends on the nature and location of the carbon on the catalyst surface.

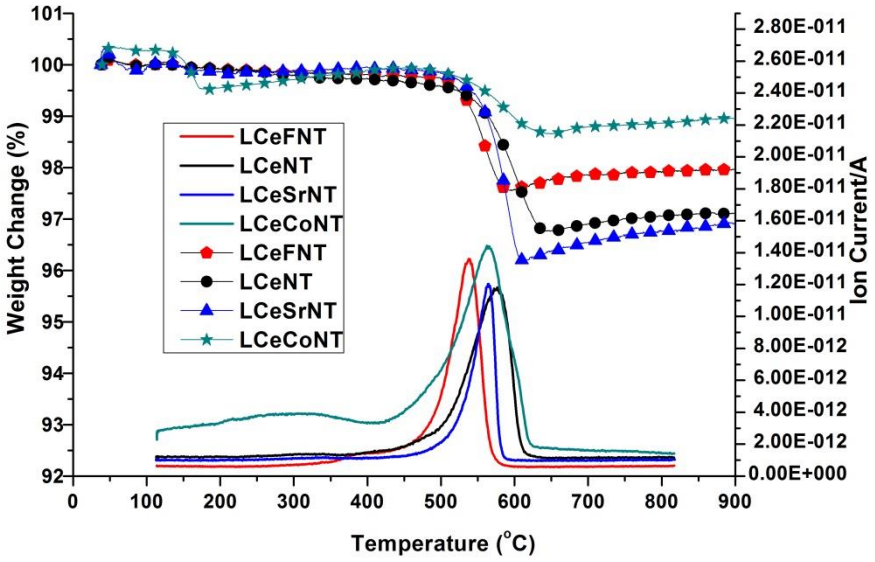

Figure 8 Oxidation of surface carbon and the corresponding change in weight of the used metal substituted A-site deficient titanate perovskite in oxidising atmosphere monitored in parallel with resultant CO_2 as a function of temperature. The temperature at which oxidation of surface carbon occurs is indicated by the CO_2 peak which depends on the nature and location of the carbon whilst the TGA profile shows the extent of coking.

Evidently, the gentle weight loss of the TGA profile suggests that all the catalyst have shown resistant and suppression of carbon deposition and suffered only a mild coking activities which corroborates reported behaviour of catalyst systems prepared by exsolution [22,62,63]. Highest weight loss of 3.56% (0.72mg) and 2.80% (0.99 mg) was observed for $La_{0.6}Ce_{0.05}Sr_{0.1}Ni_{0.1}Ti_{0.9}O_{3-\delta}$ and $La_{0.8}Ce_{0.1}Ni_{0.4}Ti_{0.6}O_{3-\delta}$ respectively attributable to their high nickel populated surfaces resulting from their robust exsolution which attracted much surface C-C and C-O bond cleavages and formation of other products. It is also interesting to observe that the catalysts systems $La_{0.7}Ce_{0.1}Co_{0.3}Ni_{0.1}Ti_{0.6}O_{3-\delta}$ and $La_{0.7}Ce_{0.1}Fe_{0.3}Ni_{0.1}Ti_{0.6}O_{3-\delta}$ that formed alloy of Co-Ni and Fe-Co respectively have shown superior stability to coking activities than the mono-metal exsolved catalysts used in this work. This observation favourably compares with the findings reported in related work [24,58]. The CO_2 peaks which indicates the temperature at which bulk of the carbon was oxidised depending upon the nature and location of the carbon on catalyst surface shows that oxidations occurred at 500-600 ^oC in all the catalysts. This suggests polymeric or graphitic carbon deposited at metal-support interphase though $La_{0.7}Ce_{0.1}Co_{0.3}Ni_{0.1}Ti_{0.6}O_{3-\delta}$ and $La_{0.7}Ce_{0.1}Fe_{0.3}Ni_{0.1}Ti_{0.6}O_{3-\delta}$ are at lower temperature relatively which indicates traces of easy-to-oxidise amorphous carbon deposited on the catalyst metal surface as a results of their peculiar properties.

Generally, all the catalysts have demonstrated good ability to supress carbon deposition activities that could lead to deactivation. This is attributed to the lattice A-site deficiency and ceria's basic-acidic as well oxygen storage-release properties that enhanced oxygen mobility and other surface properties that facilitated the oxidation of carbonaceous decomposition products that could cause carbon deposition. The titanates used as support has added extra stability and redox properties that enhanced oxidation of carbon residues from glycerol decomposition on the catalyst surfaces and suppression of coking activities which similarly compares with a related work [22] . Although the correlation between the coking activity and A-site deficiency or defect amongst the catalyst systems is not exhaustive from this work, however it compares with other related work that have shown defect due to A-site deficiency enhances oxygen mobility in the lattice which

facilitates oxidation of the carbonaceous products and therefore limits carbon deposition [22].

4.0 Conclusion and Future Perspective

Some new catalyst systems were designed and developed and have demonstrated high activity, stability and suppression of catalyst deactivation by sintering and carbon deposition in steam reforming of glycerol. The results has shown that enhanced B-site metal catalyst exsolution, surface morphology and other catalyst surface properties such as catalyst-support interaction, particle size and distribution for effective catalytic behaviour could be achieved through tailoring of defect chemistry and choice of A-site metal dopant ions. The doping of Ceria in the A-site of the perovskite catalyst has significantly enhanced and mediated the B-site metal catalyst (Ni, Co and Fe and corresponding alloys) exsolution compared to none ceria containing A-site metal dopants such as Ca, Sr and Cr ions. The metal catalyst were anchored and socketed on the titanate support with improved catalyst-support interaction, particle size and distribution as well as thermal stability against sintering and agglomeration. The exsolution design and ceria dopant has also enhanced the reducibility of the nickel particles catalyst and robust structural properties compared to those prepared by wet impregnation. The exsolved nano metals (Fe, Ni and Co) forms alloys and the synergic contribution of the dopant metal in the exsolved alloyed nanoparticle catalyst yielded a better catalytic behaviour, stability and suppression of carbon deposition activities than the mono-metal exsolved catalysts nanoparticles. Overstretching of doping ratio by 0.5% has also yielded robust exsolution of the nano-catalyst, good catalytic behaviour and suppression of carbon deposition due to increased defect from A-deficiency with apparent structural damage or instability. Consequently, defect chemistry due to A-site deficiency and careful selection of metal dopants could be used to design catalyst systems with enhanced robust surface properties.

Acknowledgements
I thank the Petroleum Technology Development Fund, Nigeria for funding this research and University of St Andrews, Scotland UK for the opportunity to do my PhD programme with them.

REFERENCES

1. Asif, M. and Munir, T. Energy supply, its demand and security issues for developed and emerging economies. *Renewable and Sustainable Energy Reviews* 11, 1388–1413 (2007)

2. Shekhawat, D.; Spivey, J. J.; and Berry, D. A.: *Fuel Cells: Technology for fuel Processing*. Elsevier Pg1-128 (2011)

3. Lo Faro, M.; Antonucci, V.; Antonucci, P. L. and Aricò, A. S. Fuel flexibility: A key challenge for SOFC technology. *Fuel,* 102 554–559 (2012)

4. Bentley, R. W. Global oil and gas depletion: An overview*. Energy Policy*, 30 189–205 (2002)

5. Casas, Y.; Arteaga, L. E.; Morales, M.; Rosa, E. Peralta, L. M. and Dewulf, J. Energy and energy analysis of an ethanol fuelled solid oxide fuel cell power plant *Chem. Eng. J.* 162, 3, 1057–1066 (2010)

6. Nobrega, S. D.; Galesco, M. V.; Girona, K.; de Florio, D. Z.; Steil, M. C.; Georges, S. and Fonseca, F. C. Direct ethanol solid oxide fuel cell operating in gradual internal reforming. *Journal of Power Sources* 213, 156-159 (2012)

7. Fan, L.; Tu, Z. and Chan, S.H. Recent development of hydrogen and fuel cell technologies: A review. Energy Reports, 7, 8421-8446, (2021)

8. Ahmed, S. and Krumpelt, M. Hydrogen from hydrocarbon fuel for fuel cells. *International journal of hydrogen energy*. 26, 291-301, (2001)

9. Gross, M. D.; Vohs, J. M. and Gorte, R. J. Recent progress in SOFC anodes for direct utilization of hydrocarbons*. J. Mater. Chem.*17, 3071-3077 (2007)

10. Fan, X. Burton, R. and Zhou, Y. Glycerol (by product of biodiesel production) as source for fuels and chemicals—mini review. *The Open Fuels & Energy Science Journal* 3, 17–22 (2010)

11. Liu, W.; Liu. C.; Gogoi, P. and Deng, Y. Overview of Biomass Conversion to Electricity and Hydrogen and Recent Developments in Low-Temperature Elecrochemical Approaches. Engineering, 6(12), 1351-1363 (2020)

12. Dauenhauer, P. J.; Salge, J. R. and Schmidt, L.D. Renewable hydrogen by autothermal steam reforming of volatile carbohydrates. *Journal of Catalysis* 244, 238–247 (2006)

13. Wu, G.; Zhang, C.; Li, S.; Han, Z.; Wang, T.; Ma, X. and Gong, J. Hydrogen production via glycerol steam reforming over Ni/Al_2O_3: Influence of nickel precursors. *ACS Sustainable Chem. Eng*. 1, 1052−1062 (2013)

14. Archer, A. S. and Steinberger-Wilckens, R. Systematic analysis of biomass derived fuels for fuel cells. *International Journal of Hydrogen Energy*, 43 (52), 23178-23192 (2018)

15. McIntosh, S. and Gorte, R. J. Direct hydrocarbon solid oxide fuel cells. *Chem. Rev.* 104, 4845-4865 (2004)

16. Adhikari, S.; Fernando, *S.*; Gwaltney, S. R.; Filip To, S. D.; Bricka, R. M.; Steele, P. H. and Haryanto, A. A thermodynamic analysis of hydrogen production by steam reforming of glycerol. *International Journal of Hydrogen Energy* 32, 2875 – 2880 (2007)

17. Sanchez, E. A. and Comelli, R. A. Hydrogen by glycerol steam reforming on a nickel–alumina catalyst: Deactivation processes and regeneration. *International Journal of Hydrogen Energy* 37 (19), 14740 – 14746 (2012)

18. Sun, W.; Wei, H.; An L.Y.; Jin, C.; Wu, H.; Xiong, Z., Pu, C.; and Sun, C. Oxygen vacancy mediated La1-xCexFeO3-δ perovskite oxides as efficient catalysts for CWAO of acrylic acid by A-site Cen doping. Applied Catalysis B: Environmental 2019, 15, 20-28, https://doi.org/10.1016/j.apcatb.2018.12.024

19. Yuan, B. Tao, Y., Qi, S.; Xie, A.; Luo, S. Effect of A, B-site cataion on the catalytic activity of La1-xAxMn1-yByO3 (A =Ce, B = Ni) p oxides for perovskite-type oxides for toluene oxidation. Environ Sci Pollut Res. 2022, https://doi.org/10.1007/s11356-022-24916-3

20. Kwon, O.; Joo, S.; Choi, S.; Sengodan, S. and Kim, G. Review on exsolution and its deriving forces. *J. Phys. Energy*, 2, 032001, (2020)

21. Kousi, K.; Tang, C.; Metcalfe, I.S. and Neagu, D. Emergence and Future of Exsolved Materials. *Small* 2006479, 1-27 (2021)

22. Ahmed Umar, Dragos Neagu and John T.S. Irvine. Alkaline modified A-site deficient perovskite catalyst surface with exsolved nanoparticles and functionality in biomass valorisation. *Biofuel Research Journal,* 29, 1342-1350, (2021)

23. Neagu, D., Oh, T., Miller, D.N., Menard, H., Bukhari, S.M., Gamble, S.R., Gorte, R.J., Vohs, J.M., Irvine, T.S.I. Nano-socketed nickel particles with enhanced coking resistance grown in situ by redox exsolution. Nat. Commun. 6, 8120. DOI: 10.1038/ncomms9120 (2015)

24. Papaioannou, E.I., Neagu, D., Ramli, W. K.W., Irvine, J.T.S., Metcalfe, I.S. Sulfur-tolerant exsolved Fe-Ni alloy nanoparticles for CO oxidation. *Topics in Catalysis. 62,* 1149-1156. https://doi.org/10.1007/s11244-018-1053-8, (2019).

25. Valdye, P. D. and Rodrigues, A. E. Glycerol for hydrogen production; A review. *Chem Eng. Technol*. 32(10), 1463 -1469 (2009)

26. Adhikari, S.; Farnando, S. D. and Haryanto, A.: Hydrogen production from glycerol: An update. *Energy Conversion and Management* 50, 2600-2604 (2009)

27. Lo Faro, M.; Minutoli, M.; Monforte, G.; Antomui, V. and Arico, A. S. Glycerol oxidation in solid oxide fuel cells based on Ni – perovskite electro catalyst. *Biomass and Bioenergy* 35,3,1075-1084 (2011)

28. Lin, Y. Catalytic volarization of glycerol to hydrogen and syngas. *Int. j. hydrogen energy*. 38, 2678-2700 (2013)

29. Ahmed Umar and John T.S. Irvine. Gasification of glycerol over Ni/γ-Al_2O_3 for hydrogen production: Tailoring catalytic properties to control deactivation. *Catal, Sustain. Energy*, 7, 65-74. (2020)

30. Boaro, M.; Colussi, S. and Trovarelli, A. Ceria-Based materials in hydrogenation and reforming reactions for CO_2 valorization. Front.Chem. 7:28. doi:10.3389/fchem.2019.00028 (2019)

31. Gao, N.; Cheng, M.; Quan, C. and Zheng, Y. Syngas production via combined dry and steam reforming of methane over Ni-Ce/ZSM-5 catalyst. Fuel 273, 117702 (2020)

32. Bezen, M. C. I.; Breitkopf, C.; Kolli, N. E. I.; Krafft, J. Louis, C. and Lercher, J. A. Selective modification of the acid–base properties of ceria by supported Au. *Chem. Eur. J.* 17 7095 – 7104 (2011).

33. Aneggi, E.; Boaro, M.; de Leitenburg, C.; Dolcetti, G. and Trovarelli, A. Insights into the redox properties of ceria-based oxides and their implications in catalysis. *Journal of Alloys and Compounds* 408–412 1096–1102 (2006)

34. Bunluesin, T.; Gorte, R. J. and Graham, G. W. Studies of the water-gas-shift reaction on ceria-supported Pt, Pd, and Rh: Implications for oxygen-storage properties. *Applied Catalysis B: Environmental* 15, 107-l 14 (1998)

35. Gorte, R. J. and Zhao, S. Studies of the water-gas-shift reaction with ceria-supported precious metals. *Catalysis Today* 104, 18–24 (2005)

36. N.D. Charisiou, G. Siakavelas, L. Tzounis, B.Dou, V. Sebastian, S.J. Hinder, M.A. Baker, K. Polychronopoulou, M.A. Goula, Ni/Y2O3-ZrO2 catalyst for hydrogen production through the glycerol steam reforming reaction. International Journal of Hydrogen Energy 45 (2020) 10442-10460.

37. M. S. Macedo, E. Kraleva, H. Ehrich, M.A. Soria, L.M. Madeira, Hydrogen production from glycerol steam reforming over Co-based catalysts supported on La2O3, AlZnOx and AlLaOx. International Journal of Hydrogen Energy 47 (2022) 33239-33258.

38. N.D. Charisiou, G. Siakavelas, K.N. Papageridis, A. Baklavaridis, L. Tzounis, K. Polychronopoulou, M.A. Goula. Hydrogen production via the glycerol steam reforming reaction over nickel supported on alumina and lanthana-alumina catalysts. International Journal of Hydrogen Energy 42 (2017) 13039-13060.

39. J.M. Silva, L.S. Ribeiro, J.J.M.Órfãob, M.A. Soria, L.M. Madeira, Low temperature glycerol steam reforming over a Rh-based catalyst combined with oxidative regeneration. International Journal of Hydrogen Energy 44 (2019) 2461-2473.

40. Nishihata, Y.; Mizuki, J.; Akao, T.; Tanaka, H.; Uenishi, M.; Kimura, M.; Okamoto,T. and Hamada, N. Self-regeneration of a Pd-perovskite catalyst for automotive emissions control *Nature* 418, 164-167 (2002)

41. Tanaka, H.; Uenishi, M.; Taniguchi, M.; Tan, I.; Narita, K.; Kimura, M.; Kaneko, K.; Nishihata, Y. and Mizuki, J. The intelligent catalyst having the self-regenerative function of Pd, Rh and Pt for automotive emissions control *Catalysis Today* 117, 321–328 (2006)

42. Neagu, D.; Tsekouras, G.; Miller, D. N.; Me´nard, H. and Irvine, J. T. S. *In situ* growth of nanoparticles through control of non-stoichiometry. *Nature Chemistry* 5, 916-923 (2013)

43. Dragos Neagu; Tae-Sik Oh; David N. Miller; Herve Menard; Syed M. Bukhari; Stephen R. Gamble; Raymond J. Gorte; John M. Vohs and John T.S. Irvine Nano-socketed nickel particles with enhanced coking resistance grown in situ by redox exsolution. *Nat. Commun*. 6, 8120 (2015)

44. Liu, S.; Chuang, K.T. & Luo, J-L. Double-layered perovskite anode with in situ exsolution of a Co-Fe alloy to cogenerate ethylene and electricity in a proton conduction ethane fuel cell. *ACS Catal.* 6, 760-768 (2015)

45. Dragos Neagu,; Evangelos, I. Papaioannow,; Wan K.W. Ramli,; David N. Miller,; Billy J. Murdoch.; Herve Menard.; Ahmed Umar.; Anders J. Barlow.; Peter J. Cumpson.; John T.S. Irvine and Ian Mettcalfe. Demonstration of chemistry through restructuring and catalytic activation at anchored nanoparticles. *Nature Communications*, 8:1855 DOI: 10.1038/s41467-017-01880-y, Pp. 1-8. www.nature.com/naturecommunications (2017)

46. Tsekouras, G., Neagu, D., Irvine, J.T.S. Step-Change in high temperature steam electrolysis performance of perovskite oxide cathodes with exsolution of B-site dopants. Energy Environ. Sci., 6, 256-266 (2013)

47. Trimm, D.L. Thermal Stability of Catalyst Support. Studies in Surface Science and Catalysis. 68, 29-51 (1991)

48. Andrievski, R. A. Review of thermal stability of nanomaterials. J Mater Sci, 49, 1449-1460. http://doi.org/10.1007/s10853-013-7836-1 (2014).

49. Trovarelli, A. Boaro, M. Rocchini, E. Leitenburg, C. Dolcetti, G. Some recent developments in the characterization of ceria-based catalysts. *Journal of Alloys and Compounds* 323–324 584–591 (2001)

50. Evans, C.D., Kondrat, S.A., Smith, P.J., Manning, T.D., Miedziak, P.J., Brett, G.L., Armstrong, R.D., Bartley, J.K., Taylor, S.H., Rosseinsky, M.J., Hutchings, G.J. The preparation of large surface area lanthanum based perovskite supports for AuPt nanoparticles: tuning the glycerol oxidation reaction pathway by switching the perovskite B site. Faraday Discussion, 188, 427-450 (2016)

51. Yasutake, T., Shinichi, N., Isamu, M., Shuichi, K., Kengo, S., Noboru, Y. Synthesis of manganite peroskites by reverse homogeneous precipitation

method in the presence of alkylammonium cation. Chem. Lett. 29(10) 1202-1203 (2000)

52. Lindenthal, L., Rameshan, R., Summerer, H., Ruh. T., Popovic, J., Nenning, A., Loffler, S., Opitz, A.K., Blaha, P., Rameshan, C.Modifying surface structure of perovskite-based catalysts by nanoparticle exsolution. Catalyst, 10(268), 2-14 (2020).

53. Afzal, S., Quan, X., Zhang, J. High surface area mesoporous nanocast $LaMO_3$ (M= Mn, Fe) perovskite for efficient catalytic ozonation and an insight into probable catalytic mechanism. Appl. Catal B: Environ., 206: 692-703 (2017)

54. Chen, C., Meng, Z. Wang, Z. Large specific surface area macroporous nano catalyst LaFe1-xNixO: A stable catalyst for catalytic methane dry reforming. Hindawi Journal of Chemistry, 1-9 (2019)

55. Merkulov, R., Samigullin, R.R., Markov, A., Patrakeev, M.V. Impact of A-site Cation deficiency on charge transport in La0.5-xSr0.5FeO3-d. Materials 2021, 14, doi:10.3390/ma14205990.

56. Nguyen, T.L., Dokiya, M., Wang, S. Tagawa, H., Hashimoto, T. The effect of oxygen vacancy on the oxide ion mobility in $LaAlO_3$-based oxides. Solid State Ionics 2000, 130m 229-241.http://dx.doi.org/10.1016/S0167-2738(00)00640-8.

57. Tang, C.; Kousi, K.; Neagu, D., and Metcalfe, I.S. Trends and progress in bimetallic exsolution. Chem. Eur. J. 10.1002/chem.202004950 (2021)

58. Tsiotsias, A.I.; Charisiou, N.D.; Yentekakis, I.V. and Goula, M. A. Bimetallic Ni-based catalysts for CO2 Methanation: A Review. Nanomaterials 2021, 11, 28. https://dx.doi.org/10. 3390/nano11010028 (2021)

59. Cheng, C. K.; Foo, S. Y. and Adesina, A. A. Carbon deposition on bimetallic Co–Ni/Al_2O_3 catalyst during steam reforming of glycerol. *Catalysis Today* 164 268–274 (2011)

60. Bartholomew, C. H. Mechanism of catalyst deactivation. *Applied Catalysis A: General* 212, 17-60 (2001)

61. Rostrup-Nielsen, J. Mechanism of carbon formation on Ni-containing catalysts. *J. Catal*. 48, 1-3, 155-165 (1977)

62. Sun, Y., Li, J., Zhang, Y., Hua, B., Luo, J. Bifunctional catalyst of core-shell nanoparticles socketed on oxygen-deficient layered perovskite for soot combustion: In situ observation of synergic dual active sites. ACS Catal., 6, 4, 2710-2714, DOI: 10.1021/acscatal.0008, (2016)

63. Urasaki, K.; Sekine, Y.; Kawabe, S.; Kikuchi, E.; Matsukata, M. Catalytic activities and coking resistance of Ni/perovskites in steam reforming of methane. Applied Catalysis A: General 286, 23-29, (2005)

Charisiou N.D.; Siakavelas, G.,; TZounis, L.; Dou, B.; Sebastian, V.; Hinder, S.J.; Baker, M.A.; Polychronopoulou; Goula, M.A. Ni/ Y_2O_3- ZrO_2 catalyst for hydrogen production through the glycerol steam reforming reaction. Int. J. hydroge. Energy. 2020, 17, 1442-10460, https://doi.org/10.1016/j.ijhydene.2019.04.237.